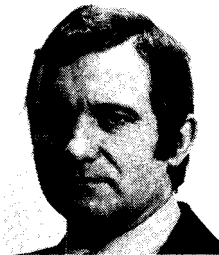


CONTINUUM DIMUON PRODUCTION BY 39.5 GEV/C
 π^\pm , K^\pm , p AND \bar{p} INCIDENT ON A TUNGSTEN TARGET

Birmingham - CERN - Ecole Polytechnique

J.D. Dowell

Physics Department, University of Birmingham



Inclusive dimuon production by 39.5 GeV/c π^\pm , K^\pm , p and \bar{p} has been studied for masses greater than 2.0 GeV/c². The π^- , π^+ and $(\pi^- - \pi^+)$ cross sections exceed the naive Drell-Yan predictions by a factor ~ 2.4 and the scaling cross section $M^3/d\sigma/dM$ scales with higher energy data within the systematic errors. The ratios of the cross sections for the different incident particles to π^- agree with Drell-Yan predictions. The pion valence structure function is consistent with that found at 200 GeV/c. Some x_F dependence of the angular distribution is observed with large errors. A comparison of $\langle P_t^2 \rangle$ at fixed τ to higher energy data shows an increase with increasing s at four values of τ .

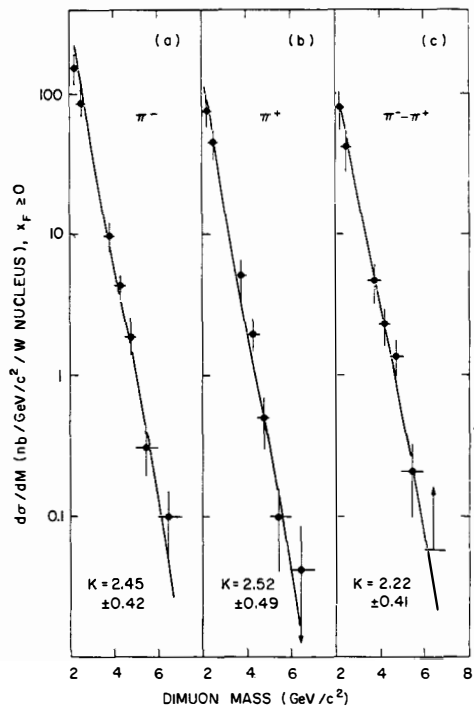


Fig. 1 $d\sigma/dM$ (nb/GeV/c²/W nucleus) for $x_F > 0$ versus mass. The curves are Drell-Yan predictions multiplied by a factor K .

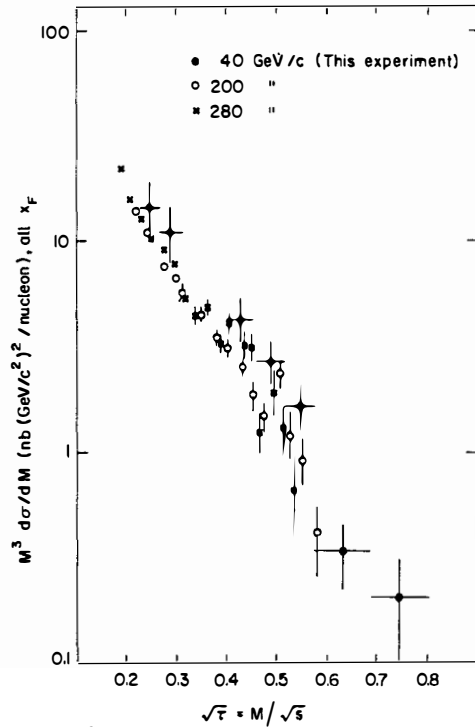


Fig. 2 $M^3 d\sigma/dM$ for all x_F as a function of $\sqrt{\tau} = M/\sqrt{s}$ for incident π^- in this experiment and ref [10]. Overall systematic errors are shown for the 40 GeV data.

The experiment was carried out in the CERN Omega Spectrometer which has a large acceptance ($-0.5 < x_F < 1.0$) for the produced dimuons. Details of the experimental method may be found in reference [1] and further information about the results discussed here in reference [2]. Data were obtained for dimuon masses from 2.0 to 7.0 GeV/c^2 or $0.23 < \sqrt{s} < 0.80$. Figure 1 shows the differential cross sections ($x_F > 0$) as a function of dimuon mass for π^- , π^+ and $(\pi^- - \pi^+)$. The data are corrected for acceptance but not for Fermi-motion and the errors include all systematic effects. The curves are calculated assuming a linear A-dependence and the simple Drell-Yan formula, using the structure functions of NA3 [3] for the pion and CDHS [4] for the nucleon, but multiplied by a factor K to fit the data. The difference cross section $(\pi^- - \pi^+)$ is expected to be free from hadronic backgrounds and requires $K=2.22 \pm 0.41$ similar to the value observed in higher energy experiments [5,6,7]. The fact that the K-values obtained for π^+ and π^- separately are only about 10% higher and the good agreement with the curves indicate that dimuon production is dominated by the Drell-Yan mechanism even at the lowest masses.

Figure 2 is a plot of the scaling cross section $M^3 d\sigma/dM$ versus \sqrt{s} at all x_F for our data and those of NA3 [10] at 200 and 280 GeV . A linear A-dependence has been used to obtain the cross section per nucleon but this is not critical as the targets (W and P_t) have similar A-values. No Fermi-motion corrections have been applied in either experiment. Our data lie about 20% higher on average but we are compatible with scaling within our errors which include all systematic effects. A small deviation in the direction observed would be expected on the basis of the scaling violations observed in deep inelastic scattering.

Figure 3 shows the cross sections for different incident particles relative to π^- as a function of mass and include our J/ψ results ($2.7 < M < 3.5 \text{ GeV}/c^2$). The π^+/π^- ratio is close to unity for J/ψ production while for the continuum it decreases with increasing dimuon mass towards the value of $\frac{1}{3}$, the ratio of the squares of the annihilating valence quark charges. For the other particles the ratios fall with mass without a discontinuity at the J/ψ . This is consistent with quark model expectations. The small ratios for K^+ and p are consequences of the absence of valence \bar{u} or \bar{d} in these particles. The solid curves are computed from the

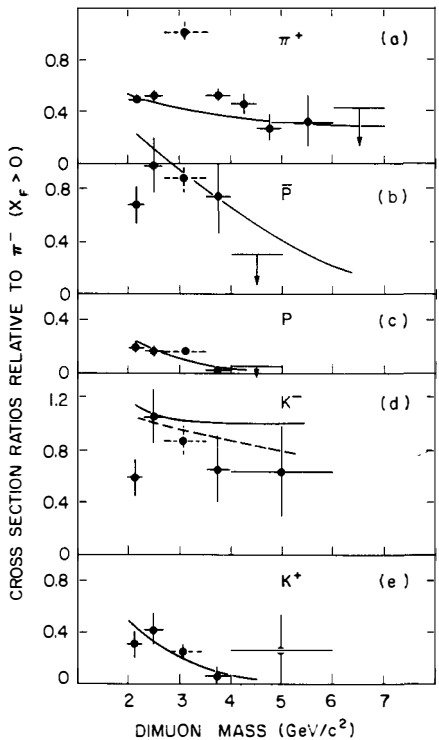


Fig. 3 Ratios for different incident particle cross sections to those for π^- . The curves are Drell-Yan predictions (see text).

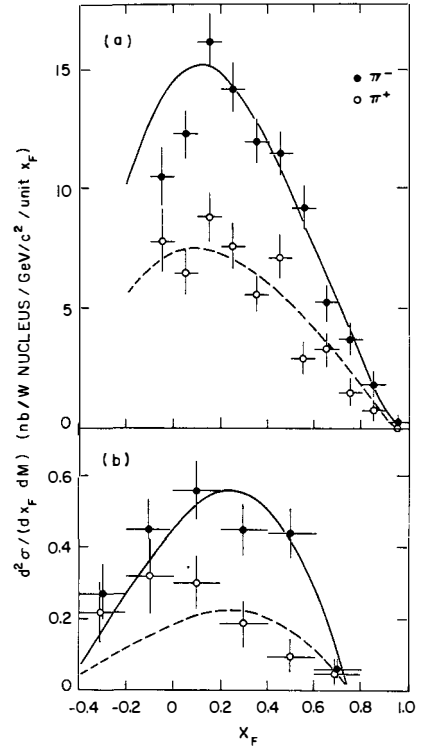


Fig. 4 $d^2\sigma/dM dx_F$ for incident π^- and π^+ , a) $2.3 < M < 2.7 \text{ GeV}/c^2$, b) $4.0 < M < 5.0 \text{ GeV}/c^2$. The curves are Drell-Yan predictions.

Drell-Yan model using the structure functions of references {3,4}. The agreement is generally good. The solid curve for K^-/π^- is where the \bar{u} distribution for the K^- is taken to be the same as for the π^- while the dashed curve uses the results of ref. {9}. for the K^- structure function. The latter agrees better with the data providing further evidence that the \bar{u} distribution in a K^- falls more steeply with x than in a π^- . The variation we observe for the K^-/π^- ratio as a function of x_F is also consistent with this result.

Figure 4a and 4b show the x_F distributions for muon pairs in the mass ranges 2.3-2.7 and 4.0-5.0 GeV/c^2 for incident π^- and π^+ . The superimposed curves (normalised to the data for $x_F > 0$) are calculated using the structure functions mentioned earlier and reproduce the data reasonably well. At higher masses the predicted x_F distributions are broader and peak further away from zero because of the difference in the valence quark distributions between pions and nucleons and the fact that large quark x -values are required to produce high masses. In order to determine the pion structure function we have fitted the data for π^+ and π^- simultaneously in the mass interval 2.0-2.7 GeV/c^2 for x_F between -0.1 and 0.8 with the pion valence structure function parameterized as $Ax^\alpha(1-x)^\beta$. The pion sea is fixed as $B(1-x)^\gamma$ where $\gamma=5$ and B is such that 6% of the pion momentum is carried by each sea quark flavour while for the nucleon the CDHS parameters have been used {4}. The fitted results give $\alpha=0.44\pm0.12$ and $\beta=0.98\pm0.15$ and a K factor of 2.6 ± 0.5 to be compared with $\alpha=0.40\pm0.06$ and $\beta=0.90\pm0.06$ in ref. {3}. There is no evidence within experimental error of any scaling violation from the shape of the pion structure function between 40 GeV/c and 200 GeV/c ; the prescription of Buras and Gaemers {8} applied to the pion predicts that the parameter β would be smaller by ~ 0.2 at the lower momentum.

The $\cos \theta$ angular distribution has been studied in the Gottfried-Jackson system for $|\cos \theta| < 0.8$ assuming that the azimuthal distribution ϕ is isotropic. The results are critically dependent on the acceptance for which a systematic error has been included. Allowance has also been made for the smearing effect of multiple scattering. The combined π^+ and π^- distributions have been fitted with $1+\cos^2\theta$. The large $|\cos \theta|$ values have the largest influence on α but are the most poorly determined because the corrections are

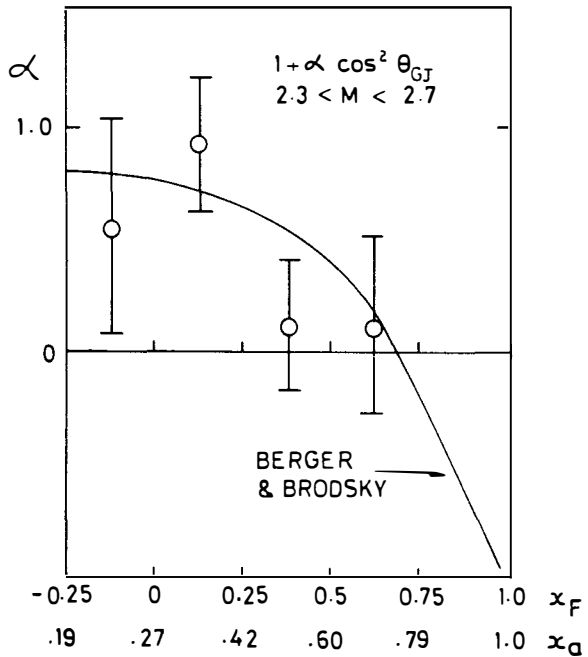


Fig. 5 The angular parameter α versus x_F for $2.3 < M < 2.7$ GeV/c 2 for π^+ and π^- data. The curve is the prediction of reference 11. The lower scale gives the x of the pion quark.

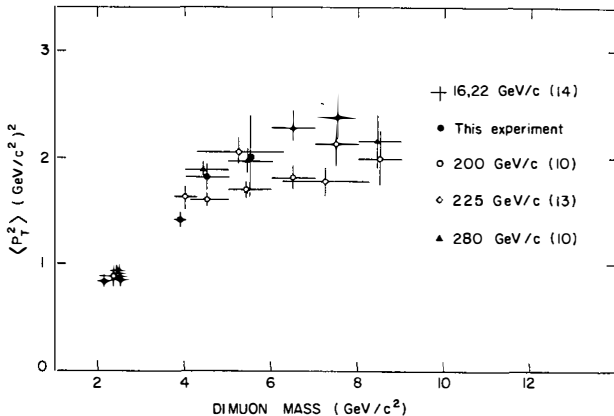


Fig. 6 $\langle p_t^2 \rangle$ versus mass for incident π^- for these and other data.

large and the statistics low. Consequently one should be cautious in interpreting the results. The values of α obtained for $x > -0.25$ are $\alpha = 0.44 \pm 0.17$ (0.44 ± 0.48) for the mass regions $2.3-2.7 \text{ GeV}/c^2$ ($4.0-5.0 \text{ GeV}/c^2$). Figure 5 is a plot of α versus x_F for the lower mass range, with the lower scale showing the x -value of the quark in the pion. The curve is the prediction of Berger and Brodsky [11] and the data show the predicted decrease in α with increasing x_F as first observed at $225 \text{ GeV}/c$ [12]. However the large errors and systematic uncertainties make it difficult to draw a conclusion.

The P_t^2 distributions for the π^- and π^+ induced dimuons are well fitted by an exponential form for $P_t^2 < 2.0 (\text{GeV}/c)^2$. At higher P_t^2 the data fall more slowly than the exponential as observed in reference [10]. The $\langle P_t^2 \rangle$ values are similar for all beam particles and show a dependence on mass and x_F . Corrections have been applied to $\langle P_t^2 \rangle$ to allow for the smearing effect of multiple scattering. Figure 6 shows $\langle P_t^2 \rangle$ versus mass compared to other data. Our data have a similar mass dependence to the higher energy data but correspond to much higher values of $\sqrt{\tau}$. Figure 7 shows $\langle P_t^2 \rangle$ versus s at four values of $\sqrt{\tau}$. There appear to be some inconsistencies but the data show that $\langle P_t^2 \rangle$ increases with s at fixed τ . The straight lines are not fits but are to guide the eye and have slopes ranging from .0023 to .0035 with no clear systematic trend. There is not a common intercept on the $\langle P_t^2 \rangle$ axis implying that the primordial $\langle P_t^2 \rangle$ is a function of τ . Our data show a smooth decrease of $\langle P_t^2 \rangle$ with increasing x_F (figure 8) which is particularly striking at high mass where it must at least partly reflect the approach to the kinematic boundary. The acceptance is a slowly varying function of both x_F and P_t and could not, due to error, account for the behaviour.

In conclusion we observe at $40 \text{ GeV}/c$ only a small change in the scaled continuum cross section $M^3 d\sigma/dM$ from the values measured at 200 and $280 \text{ GeV}/c$. The cross sections exceed the naive Drell-Yan predictions by a factor ~ 2.4 . The pion valence structure function is consistent with that found at $200 \text{ GeV}/c$. Some evidence of a dependence of the angular distribution parameter α on x_F is observed but the errors are large. Comparing to higher energy data $\langle P_t^2 \rangle$ rises with increasing s at fixed τ but decreases with x_F at our energy.

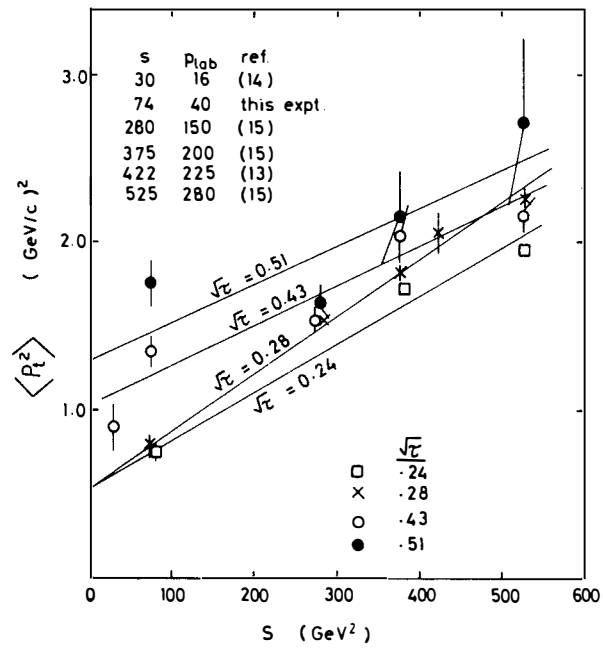


Fig. 7 $\langle p_t^2 \rangle$ versus s for incident π^- at four values of $\sqrt{\tau}$ for these and other data. The lines are to guide the eye.

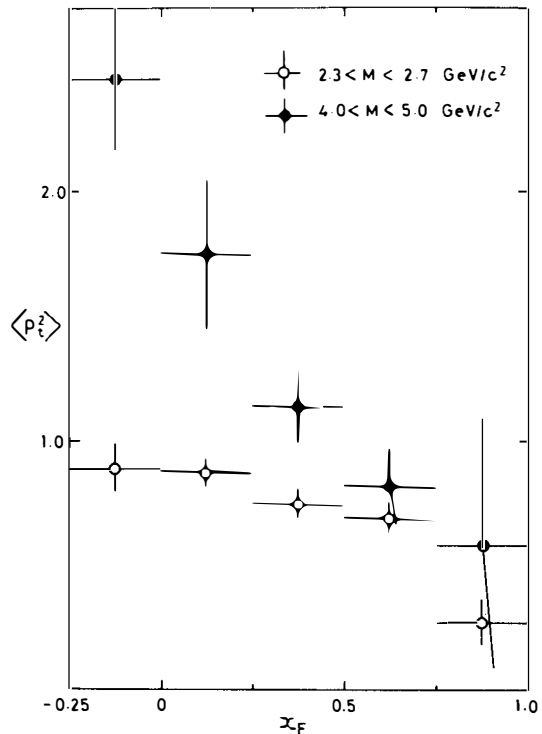


Fig. 8 $\langle p_t^2 \rangle$ versus x_F for incident π^- and two mass intervals.

References

1. M.J. Corden et al., Phys. Lett. 96B (1980) 411.
2. M.J. Corden et al., Phys. Lett. 96B (1980) 417.
and CERN/EP/80-152.
3. J. Badier et al., CERN/EP/79-67.
4. J.G.H. de Groot et al., Phys. Lett. 82B (1979) 456.
5. J. Badier et al., Phys. Lett. 89B (1979) 145.
6. R. Barate et al., Phys. Rev. Lett. 43 (1979) 1541.
7. A.S. Ito et al., Fermilab - Pub - 80/19 - Exp.
8. A.J. Buras and K.J.F. Gaemers, Nucl. Phys B132 (1978) 249.
9. J. Badier et al., Phys. Lett. 93B (1980) 354.
10. J. Badier et al., CERN/EP/79-68.
11. E.L. Berger and S.J. Brodsky, Phys. Rev. Lett. 42 (1979) 940.
12. K.J. Anderson et al., Phys. Rev. Lett. 43 (1979) 1219.
13. K.J. Anderson et al., Phys. Rev. Lett. 42 (1979) 944.
14. J. Alspector et al., Phys. Lett. 81B (1979) 397.
15. J. Badier et al., CERN/EP/80-150.

*

M.J. Corden, J.D. Dowell, J. Garvey, R.J. Homer, M. Jobes,
I.R. Kenyon, T.J. McMahon, R.C. Owen, K.C.T.O. Sumorok,
R.J. Vallance, P.M. Watkins and J.A. Wilson.

University of Birmingham, UK.

P. Sonderegger.

CERN, European Organisation for Nuclear Research, Geneva
Switzerland.

B. Chaurand, A. Romana and R. Salmeron.
Ecole Polytechnique, Palaiseau, France.